J Geod (2006)
DOI 10.1007/s00190-006-0027-y

ORIGINAL ARTICLE

A.O. Kohlhase · R. Kroes · S. D'Amico

Interferometric baseline performance estimations for multistatic synthetic aperture radar configurations derived from GRACE GPS observations

Received: 18 April 2005/ Accepted: 23 January 2006

Abstract Recent studies have demonstrated the usefulness of global positioning system (GPS) receivers for relative positioning of formation-flying satellites using dual-frequency carrier-phase observations. The accurate determination of distances or baselines between satellites flying in formation can provide significant benefits to a wide area of geodetic studies. For spaceborne radar interferometry in particular, such measurements will improve the accuracy of interferometric products such as digital elevation models (DEM) or surface deformation maps. The aim of this study is to analyze the impact of relative position errors on the interferometric baseline performance of multistatic synthetic aperture radar (SAR) satellites flying in such a formation. Based on accuracy results obtained from differential GPS (DGPS) observations between the twin gravity recovery and climate experiment (GRACE) satellites, baseline uncertainties are derived for three interferometric scenarios of a dedicated SAR mission. For cross-track interferometry in a bistatic operational mode, a mean 2D baseline error (1σ) of 1.4 mm is derived, whereas baseline estimates necessary for a monostatic acquisition mode with a 50 km along-track separation reveal a 2D uncertainty of approximately 1.7 mm. Absolute orbit solutions based on reduced dynamic orbit determination techniques using GRACE GPS code and carrier-phase data allows a repeat-pass baseline estimation with an accuracy down to 4 cm (2D 1σ). To assess the accuracy with respect to quality requirements of high-resolution DEMs, topographic height errors are derived from the estimated baseline uncertainties. Taking the monostatic pursuit flight configuration as the worst case for baseline performance, the analysis reveals that the induced low-frequency modulation (height bias) fulfills the relative vertical accuracy requirement ($\sigma < 1$ m linear point-to-point error) according to the digital terrain elevation data level 3 (DTED-3) specifications for most of the baseline constellations. The use of a GPS-based reduced dynamic orbit determination technique improves the baseline performance for repeat-pass interferometry. The problem of fulfilling the DTED-3 horizontal accuracy requirements is still an issue to be investigated. DGPS can be used as an operational navigation tool for high-precision baseline estimation if a geodetic-grade dual-frequency spaceborne GPS receiver is assumed to be the primary instrument onboard the SAR satellites. The possibility of using only single-frequency receivers, however, requires further research effort.

Keywords Multistatic synthetic aperture radar (SAR) interferometry · Close formation-flying satellites · Relative GPS positioning · Baseline performance analysis · Digital elevation model (DEM)

Deutsche Forschungsgemeinschaft (DFG) research fellow until Sept. 2004 at the Microwaves and Radar Institute, Deutsche Zentrum für Luft- und Raumfahrt (DLR) e.V., 82234 Weßling, Germany

A.O. Kohlhase (✉) · S. D'Amico
German Space Operations Center (GSOC), DLR e.V.,
Münchner Straße 20, 82234 Weßling, Germany
E-mail: andreas.kohlhase@dlr.de
E-mail: simone.damico@dlr.de
Tel.: +49-8153-282106
Fax: +49-8153-281455
Tel.: +49-8153-282115
Fax: +49-8153-281450

R. Kroes
Department of Earth Observation and Space Systems (DEOS),
TU Delft, Kluywerweg 1, 2926 Delft, The Netherlands
E-mail: r.kroes@lr.tudelft.nl
Tel.: +31-15-2786221
Fax: +31-15-2785322

1 Introduction

The accurate digital mapping of the world's topography using synthetic aperture radar (SAR) interferometry is still a major topic in Earth remote sensing (e.g., Zebker et al. 1994a; Moreira et al. 2004). This geodetic technique is based on the combination of two SAR images of the same scene acquired from slightly different positions in space to measure a phase difference in each co-registered pixel. The measured interferometric phase can be used to derive topographic height information on the imaged terrain and thus to generate a digital elevation model (DEM) (e.g., Rodriguez and Martin 1992). The precision of the height estimation is primarily deter-

mined by the size of the satellite-to-satellite baseline distance and the accuracy of its reconstruction, as well as the quality of the interferometric phase correlation. During the Shuttle radar topographic mission (SRTM), e.g., the interferometric performance was limited by the fixed 60 m boom (Werner 2001).

The baseline length is one of the main driving parameters for the performance of SAR and mainly determines the vertical accuracy of the estimated DEM. A solution to overcome this problem is thus to define a satellite constellation that allows for varying and multiple baselines to acquire two or more SAR images of the same scene quasi-simultaneously. In addition, if one SAR sensor is transmitting and receiving, whereas the other ones only receive the radar echoes, the interferometric measurement becomes less sensitive to phase ambiguities. This approach is called multistatic single-pass SAR interferometry.

An important parameter to quantify the sensitivity is the so-called height or altitude of ambiguity. This height corresponds to exactly one interferometric phase cycle $[0, 2\pi]$ of range change between the SAR sensor and a reflector on the ground. In other words, if a terrain elevation exceeds the altitude of ambiguity, the measurement becomes ambiguous. The principal observation is thus a 2D relative phase signal, which is the 2π-modulus of the (unknown) absolute phase signal (Hanssen 2001).

To solve the integer ambiguity number in each pixel, the approach of 'phase unwrapping' of interferometric SAR (InSAR) data has to be applied. This approach is based on the integration of the phase gradients, e.g., simply by a 1D (flood-fill) summation of the phase gradients, starting from an arbitrary seed location. Conventional methods for phase unwrapping are, e.g., discussed by Bamler and Hartl (1998) and Goldstein et al. (1998). As an excellent reference for the investigation of multistatic SAR formation flights and their performances, we refer to Evans et al. (2002), Martin et al. (2001), Massonnet (2001), Krieger et al. (2003) and Zink et al. (2003). Along with other disturbing effects, the accurate and operational baseline determination during a multistatic SAR mission remains a significant problem for the generation of world-wide and consistently high-precision DEMs.

An alternative way of baseline refinement is a tie-point or DEM-based baseline optimization. Tie-points are natural or artificial radar targets in the SAR image that stand out clearly from the signal of the background backscattering. For example, the power difference between a corner reflector and its surrounding area is about 18 dB (Hanssen 2001). Tie-points can be manually localized in the interferogram amplitude using a topographic reference map. In order to improve baseline knowledge, the tie-points have to be identified and used along with the unwrapped phase to solve the equations for baseline refinement (Padia et al. 2002). In case of an unwrapping failure, existing DEMs can be used as a priori information on the unwrapped phase.

To have the opportunity of flexible baseline selection and to counteract the problem of the inherent accuracy limitation due to temporal decorrelation and atmospheric disturbances, a bistatic tandem mission has recently been proposed, where a second SAR satellite shall fly in close formation with the first one (Moreira et al. 2004). The nominal SAR acquisition mode is bistatic, i.e., the SAR instrument of the master satellite will be active (transmitting and receiving), whereas the one on the slave satellite will be passive (only receiving). The main mission goal is to generate high-resolution DEMs on a global scale as a basis for a wide range of scientific research, as well as for operational and commercial DEM production. The proposed bistatic mission combines the advantages of the tri-nodal pendulum (Fiedler and Krieger 2004; Zink et al. 2003) with those of the cartwheel concept proposed earlier (Massonnet 2001).

To analyze the performance of a multistatic SAR system comprehensively, we need to estimate the interferometric phase and baseline errors. Both errors can be propagated into so-called topographic or interferometric height errors, which determines the vertical resolution and precision of a DEM. For multistatic SAR configurations, the influence of interferometric phase errors on the height accuracy has already been analyzed by Krieger et al. (2003). However, the specific performance under the condition of rapidly changing multistatic baseline conditions requires a detailed analysis in so far as the achievable baseline accuracy changes for different baseline determination strategies.

In this paper, we analyze and assess the capability to achieve a stated DEM accuracy requirement by deriving height biases from baseline errors. We use GPS positioning results from the global recovery and climate experiment (GRACE) mission (e.g., Tapley et al. 2004b) to estimate the baseline errors for different interferometric scenarios of a dedicated SAR mission. Here, the availability of the K-band radar link provides a unique operation for validating GPS-based relative positions at the sub-mm level. In this way, realistic accuracy estimates can be derived that are free of simplifying assumptions made in earlier software and hardware-in-the-loop simulation (Kroes and Montenbruck 2004a).

2 Performance requirements and basic assumptions

To analyze the baseline performance of an exemplary multistatic SAR interferometer in more detail, we use the main system specifications of the proposed TanDEM-X mission (Moreira et al., 2004) in which two main interferometric scenarios are defined for DEM generation: the bistatic operational mode as described in the previous section and the monostatic pursuit mode in which one satellite pursues the other with a selectable along-track separation. This ensures independent active work of both instruments, i.e., both SAR antennas will transmit and receive. Furthermore, a repeat-pass scenario for the prime satellite TerraSAR-X is taken into account. A brief review of the mission and system requirements, its operational modes, as well as the commercial and scientific applications are given in Moreira et al. (2004). Werninghaus et al. (2004) outline the different SAR acquisition capabilities of the TerraSAR-X satellite.

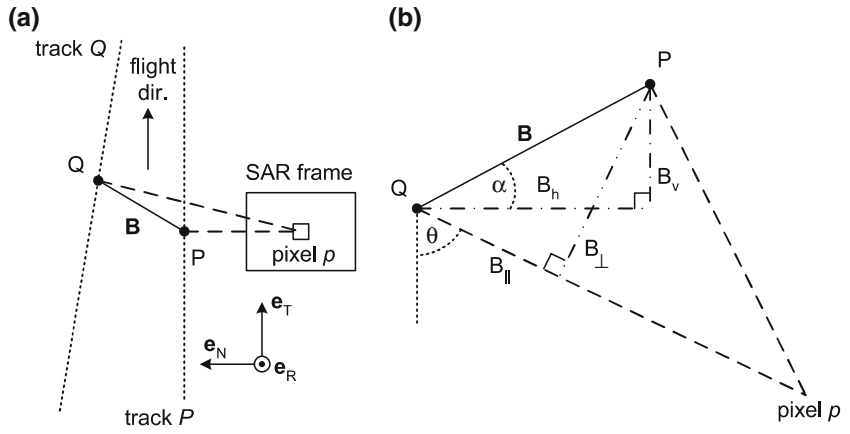

Fig. 1 **a** The baseline is formed at the moment of alignment of a co-registered pixel p. Here, points P and Q resemble the positions of the spacecraft at the moment of alignment for the different scenarios, listed in Table 1. **b** Two possible representations of the interferometric baseline: horizontal/vertical or parallel/perpendicular

Table 1 Physical representation of the points P and Q in Fig. 1 for the different interferometric scenarios

Scenario	P		Q	
	Spacecraft	Epoch	Spacecraft	Epoch
Bistatic	A	t_0	B	t_0
Monostatic pursuit	A	$t_0 + \Delta t$	B	t_0
Repeat-pass	A	t_1	A	t_2

2.1 Definition of baseline geometry

The baseline geometry for the two SAR acquisition modes and for the repeat-pass scenario is explained using Fig. 1. Here points P and Q resemble the different spacecraft positions for each scenario at the moment when the co-registered pixels of the SAR frames are aligned (Fig. 1a). The baseline

$$\mathbf{B} = [B_R \; B_T \; B_N]^{\mathrm{T}} \tag{1}$$

is a 3D relative position between these points and is usually defined in the co-rotating coordinate system, in which the unit vector $\mathbf{e}_{\mathrm{R}}$ points in radial, $\mathbf{e}_{\mathrm{T}}$ in tangential (along-track), and $\mathbf{e}_{\mathrm{N}}$ in normal (cross-track) direction (Fig. 1a). $\mathbf{B}$ thus consists of a radial, B_{R}, an along-track, B_{T}, and a cross-track component B_{N}.

The baseline can be displayed in a 2D plane stretched between the pixel p and points P and Q (Fig. 1b). It can be subdivided into a horizontal, B_{h}, and a vertical component, B_{v}, or into a parallel, $B_{\parallel}$, and perpendicular component $B_{\perp}$. $B_{\perp}$ is also referred to as the effective baseline. Both baseline representations may simply be converted to each other by using the radar look angle θ, which is defined with respect to the geocentric state vector of a spacecraft at point Q. The attitude or tilt angle α is used to describe the orientation of the baseline with respect to the horizon. The exact meanings of points P and Q for the different scenarios can be found in Table 1 and are discussed in detail in the next subsection.

In this study, the estimation of the baseline error is the primary concern. Baseline errors in the tangential direction, $\sigma_{B_{\mathrm{T}}}$, are usually corrected for sufficiently during SAR frame alignment (Hanssen 2001). Only the errors in cross-track and radial direction propagate as phase errors into the interferogram, making it essentially a 2D problem. In the following, the (B_{N}, B_{R})-representation is used since errors in the horizontal and vertical component of the baseline can directly be related to the cross-track and radial orbit errors, respectively. Hence

$$\sigma_{B_{\mathrm{N}}} = \sigma_{B_{\mathrm{h}}} \quad \text{and} \quad \sigma_{B_{\mathrm{R}}} = \sigma_{B_{\mathrm{v}}} \tag{2}$$

2.2 Fundamentals of the three SAR acquisition modes

Basically, the differencing of two SAR images acquired in the cross-track direction yields the measurement of terrain elevations. In this case, two SAR images of the identical spot are taken by the *same* instrument. Points P and Q in Fig. 1 therefore resemble the same spacecraft (A in this case) at epochs t_1 and t_2, respectively. For the TerraSAR-X mission, the time interval between two repeat passes, t_2–t_1, is planned to be exactly 11 days. In the bistatic scenario, the SAR images are acquired by two different instruments at the same instant t_0. One antenna transmits and receives while the other only receives. Therefore points P and Q represent spacecrafts A and B, respectively, and the baseline is identical to the physical relative position between both spacecrafts.

In contrast, along-track interferometry (ALI) is not based on a certain interferometric baseline, but on a small time lag between two moving SAR instruments separated in along-track direction and imaging the same terrain (Gill and Runge 2004). This provides measurements of the line-of-sight velocity of objects on the ground. The measured phase difference is a function of the target velocity, the radar wavelength and the antenna separation. Consequently, the along-track separation has to be 'adjusted' in such a way that the processing allows for the detection of corresponding velocities of on-ground objects.

In the monostatic pursuit mode, the along-track separation will be in the order of 30–50 km to acquire independent

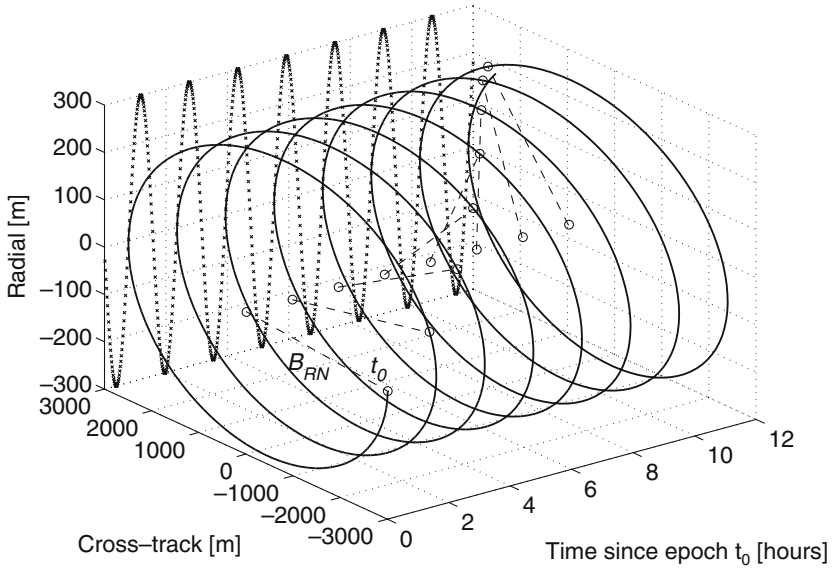

Fig. 2 3D representation of motion of the baseline vector $\mathbf{B}_{\mathrm{RN}}$. Here, the baseline is expressed as a 2D vector formed by the radial and cross-track component of the differenced state vectors at epoch t. The baseline is plotted as a function of constant time steps since t_0 demonstrating the characteristic helical rotation

SAR data for DEM generation. The corresponding time difference of the SAR acquisitions is $\Delta t \approx 4$–7 s. The distance variation has to account for two antagonistic effects: long along-track separations to exclude any interference between the radar instruments and short separations to avoid temporal decorrelation. The advantage of the monostatic acquisition mode is that there is no need for phase synchronization. However, the height sensitivity for phase unwrapping is doubled with respect to multistatic operation, and the small temporal separation slightly reduces the accuracy of the baseline estimation, which will be shown in Sect. 3.3.

2.3 DEM vertical accuracy requirements

Baseline errors tend to create an overlaid artifact of a 'phase ramp' in the interferogram with a constant, long-wavelength gradient in a certain direction (Kohlhase et al. 2003). This, in turn, will mainly cause a low-frequency modulation of the DEM, thereby contributing simultaneously to relative and absolute height errors (Krieger et al. 2004). This means that the baseline-induced height bias screen has to be compliant with the relative vertical accuracy according to the digital terrain elevation data level 3 (DTED-3) specifications, which is claimed for the TanDEM-X mission.

The stated accuracy objective is <2 m linear point-to-point error at 90% probability for flat terrains. This allows the assumption of a relative vertical accuracy of roughly <1 m linear point-to-point error at 68.3% (1σ) probability. Since the radar is always side-looking, terrain elevation will result in geometric distortions in the SAR image due to the varying incidence angle (Hanssen 2001).

To find a trade-off between a high signal-to-noise ratio (SNR) and reduced distortion effects, the SAR satellites will map the scene under different radar look angles, which also has to be accounted for in the performance analysis. For the analysis presented here, it is assumed that errors in the interferometric phase and bistatic focusing can be modeled precisely, which is important for the separation between the baseline and purely phase-noise-induced height bias in each DEM point.

2.4 Prediction of relative motion

In order to predict the relative motion of two satellites in space and thus to have a priori information of the baseline vector, a possible approach is to numerically integrate the differential equations of motion of both objects in the presence of all relevant perturbations (Montenbruck and Gill 2000). We choose the initial values in such a way that the characteristic formation flight is reached as described in D'Amico and Montenbruck (2006). To minimize the risk of collision, care is taken to properly separate the two spacecrafts in radial and cross-track directions. This is achieved by a parallel (or anti-parallel) alignment of the relative eccentricity and inclination vectors.

Both TanDEM-X satellites will orbit the Earth in nearly circular and sun synchronous orbits. A difference in the right ascension of the ascending nodes ensures a horizontal offset in the equatorial region, whereas a slight difference in the eccentricities allows for a minimal vertical displacement in polar regions. The 2D baseline vector is simply formed by using the radial/cross-track representation of the differenced state vectors at a certain epoch. This prediction yields a baseline length of roughly 300 m for the vertical attitude ($\alpha = 90°$) and 3000 m for the horizontal orientation ($\alpha = 0°$); see Fig. 2. The dynamical behavior of the resulting interfer-

ometric baseline can be characterized by a so-called helix rotation with a fluctuating length.

As shown in D'Amico and Montenbruck (2006), such a formation-flying configuration is naturally stable over short-term prediction arcs (i.e., hours). For long-term formation flying (i.e., days), a relative orbit control of the formation is necessary in order to counteract differential perturbations mainly caused by the Earth's oblateness (i.e., J_2 effects) and differential atmospheric drag.

3 Performance of baseline determination strategies

Over the past few years, GPS has been demonstrated as a successful method for precise orbit determination (POD) of satellites such as CHAMP (van den IJssel and Visser 2003), Jason-1 (Haines et al. 2002) and GRACE (Montenbruck et al. 2004) with accuracies better than 10 cm. GPS provides the ability for both real-time navigation solutions and highly accurate post-facto orbit reconstruction. In addition, GPS can also be used for highly accurate time synchronization (Parker and Matsakis 2004) for onboard applications.

In the following, the obtainable baseline accuracy for the three different interferometric scenarios is assessed using realistic GPS POD results obtained from the GRACE mission. A geodetic-grade dual-frequency spaceborne GPS receiver, such as the JPL BlackJack GPS receiver (Montenbruck and Kroes 2003), is assumed to be the primary instrument for POD onboard the SAR satellites.

The GRACE mission consists of two identical formation-flying satellites in a near-polar near-circular orbit with an altitude of approximately 450 km. The satellites have a nominal along-track separation of around 220 km (Tapley et al. 2004a). The primary mission objective is to measure the time-varying changes in the Earth's gravitational field (Tapley et al. 2004a), which is accomplished in part by the mission's key instrument, the K-band inter-satellite ranging system (KBR). This instrument measures the change in distance (biased range) between both satellites with a precision better than 10 μm. Both satellites are equipped with a modified version of the BlackJack GPS receiver, which also serves as an instrument processing unit (IPU). In addition to making the usual GPS observations, it also processes the star camera and KBR signals. An review of the entire GRACE mission can be found in NASA (2003).

3.1 Repeat-pass interferometry

Since the same satellite takes SAR images after a defined repeat cycle, the interferometric baseline

$$\mathbf{B} = \mathbf{r}_\mathrm{A}(t_2) - \mathbf{r}_\mathrm{A}(t_1) \tag{3}$$

is thus formed from two absolute positions (Fig. 1) of the satellite at epochs t_1 and t_2. The baseline error

$$\epsilon_\mathbf{B} = \epsilon_{\mathbf{r}_\mathrm{A}}(t_2) - \epsilon_{\mathbf{r}_\mathrm{A}}(t_1) \tag{4}$$

results from the individual errors of both satellite passes. For long time-scales, there is no temporal correlation between the errors of the repeat-pass position vector $\mathbf{r}_\mathrm{A}$. The inaccuracies of both absolute positions are simply propagated into the uncertainty of the baseline length

$$\sigma_\mathrm{B} = \sqrt{\sigma^2_{\mathbf{r}_\mathrm{A}}(t_2) + \sigma^2_{\mathbf{r}_\mathrm{A}}(t_1)} = \sqrt{2}\,\sigma_{\mathbf{r}_\mathrm{A}}. \tag{5}$$

Realistic accuracies for GPS-based absolute orbits are obtained from an orbit comparison of the GRACE mission found in Table 2, which shows the difference between the absolute orbit solutions computed for this study at the Deutsches Zentrum für Luft- und Raumfahrt (DLR) and the Jet Propulsion Laboratory (JPL) solutions of GRACE A and B, respectively, in radial, along-track and cross-track directions. The JPL orbit solution is distributed with the publicly available GRACE data (Case et al. 2002). The DLR orbits have been computed using the reduced dynamic batch least-squares estimation process (Montenbruck et al. 2004), using both GPS code pseudorange and carrier-phase data. The difference among solutions from several institutes gives a good indication of the overall orbit accuracy. Here, the overall orbital errors are obtained as roughly 2 cm in the radial and cross-track directions and 4 cm in the along-track direction.

Expressing Eq. 5 in terms of mean uncertainties in radial and cross-track directions, a 2D baseline uncertainty

$$\sigma_\mathrm{B} = \sqrt{2\,(\bar{\sigma}^2_R + \bar{\sigma}^2_N)} \tag{6}$$

of 4.3 cm may be estimated for a repeat-pass scenario using absolute GPS navigation solutions for post-facto orbit reconstruction.

3.2 Bistatic operational mode

For this scenario, the interferometric baseline

$$\mathbf{B} = \Delta\mathbf{r}_\mathrm{DGPS}(t_0) \tag{7}$$

is identical to the observation of relative position between both satellites according to Fig. 1. A study by Kroes et al.

Table 2 Comparison of absolute orbit solutions for GRACE A and B computed at DLR and JPL for 2003 DOY 210 - 220 (July 29–August 8)

Doy	Grace A / B		
	σ_R(cm)	σ_T(cm)	σ_N(cm)
210	2.1/2.2	3.9/3.8	2.1/1.9
211	2.3/2.3	4.1/4.1	2.2/2.1
212	2.4/2.7	4.3/4.5	1.8/1.6
213	2.1/2.2	3.3/3.8	2.7/1.8
214	2.2/2.3	4.2/4.1	2.9/1.8
215	2.0/2.3	3.8/4.1	2.7/2.2
216	2.1/2.2	4.2/4.1	2.4/1.8
217	1.9/2.1	3.2/3.5	2.7/2.0
218	2.2/2.1	4.0/3.9	2.0/1.9
219	1.9/2.3	3.4/4.0	2.5/1.7
220	1.9/2.3	3.1/4.0	1.9/1.8
Avg.	2.2	3.9	2.1

Table 3 Comparison of the relative orbit solution for GRACE A and B, from the absolute orbits and by direct differential GPS processing

DOY	GPS (DLR - JPL)			GPS (JPL - KBR)	GPS (DLR - KBR)	DGPS (DLR - KBR)
	σ_R(mm)	σ_T(mm)	σ_N(mm)	σ_T(mm)	σ_T(mm)	σ_T(mm)
210	10.3	24.0	14.6	16.1	14.4	1.03
211	13.6	24.7	15.0	17.6	15.9	0.82
212	10.5	22.5	13.8	17.7	14.5	0.81
213	11.2	21.5	20.1	16.4	10.6	1.20
214	10.9	24.6	27.3	16.0	13.3	0.86
215	13.4	30.5	16.2	16.4	22.6	1.03
216	9.1	36.7	18.8	18.3	21.0	0.72
217	11.1	23.2	19.9	17.6	13.9	1.41
218	9.9	21.7	14.6	18.3	13.8	0.95
219	11.5	22.1	26.0	19.5	12.1	0.81
220	12.7	26.1	22.5	17.8	16.9	1.19
Avg.	11.3	25.2	19.0	17.4	15.4	0.98

Columns 2, 3 and 4 show the radial, along-track, and cross-track errors of the DLR relative position minus the one of the JPL, both formed by subtracting the absolute positions. Columns 5 and 6 show the error of the DLR and JPL relative position, again from absolute positions, with respect to the KBR observations (along-track). The results of relative position, directly computed using DGPS data, in comparison to the KBR are shown in the last column. They are based on Kroes et al. (2004b)

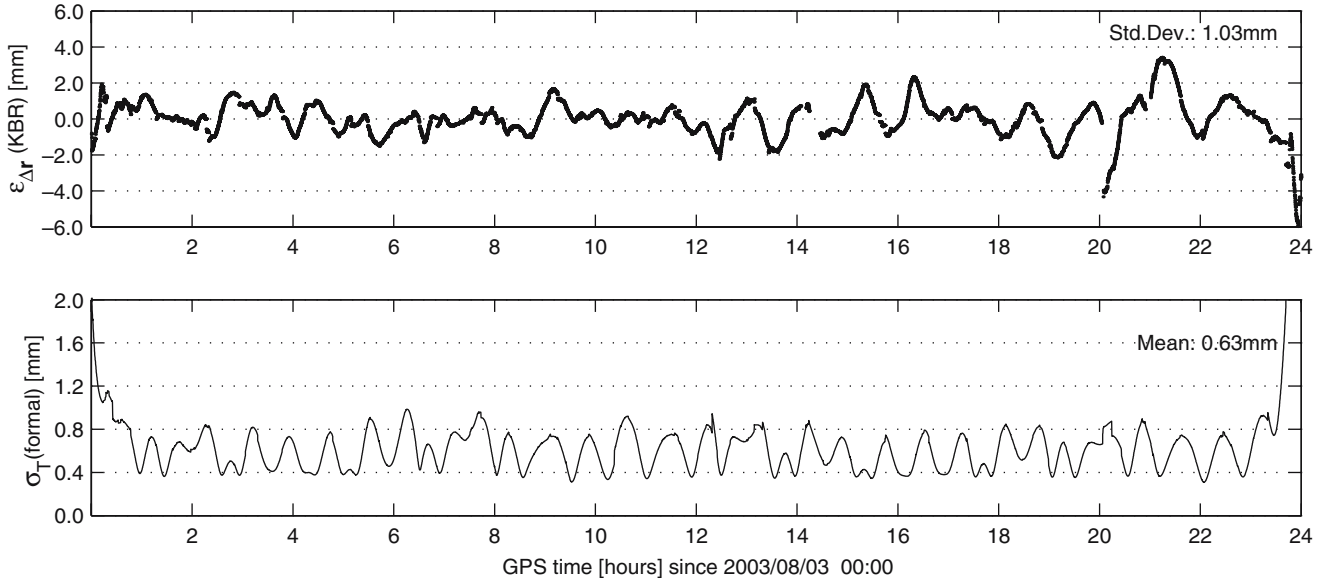

Fig. 3 For 2003 DOY 215: *top* true GRACE relative position error, $\epsilon_{\Delta \mathbf{r}}$, from the DGPS filter verified using KBR data. *Bottom* the formal DGPS filter along-track error (1σ)

(2004b) using data from the GRACE mission has shown that DGPS can also be successfully applied for precise relative positioning of formation-flying satellites. The unique aspect of the GRACE mission is that the accuracy of the along-track component of the relative position can be verified precisely with data from the KBR. Table 3 shows the uncertainties of the GRACE relative position compared to KBR data. For completeness, the relative position has been computed directly using DGPS data and by simply subtracting the absolute positions of both spacecrafts.

As can be seen from Table 3, the direct processing of DGPS data yields the highest accuracy of typically 1 mm in along-track direction. Simply subtracting two individual absolute orbit solutions does not give the desired accuracy, but still shows that the orbit errors of the individual satellites are highly correlated within the formation. This can be seen by comparing the accuracies in Tables 2 and 3, where particularly, the difference in the uncertainty of the along-track component is clearly visible.

Figure 3 shows the error of the GRACE relative position, $\epsilon_{\Delta \mathbf{r}}$, estimated using the DGPS filter described in Kroes et al. (2004b) in comparison with data from the KBR. Also shown in Fig. 3 is the filter formal error in along-track direction. The 1σ value of the true error is 1 mm, which is close to the filter prediction of 0.6 mm. The DGPS filter shows the same formal error for the radial, along-track, and cross-track direction. It is therefore assumed that the true error for each component is also identical for all axes, resulting in a mean 2D baseline uncertainty

$$\sigma_B = \sqrt{\bar{\sigma}^2_{\Delta r_R} + \bar{\sigma}^2_{\Delta r_N}} = \sqrt{2}\,\bar{\sigma}_{T,\mathrm{DGPS}} \tag{8}$$

of 1.4 mm for a bistatic scenario.

Since the relative distance of the TanDEM-X satellites in the bistatic formation flight is much smaller (<3 km) than for GRACE (∼220 km), an increase in baseline accuracy might be expected. However, this is not the case since the baseline solution is most likely dominated by errors independent of the separation, such as GPS signal multipath. A shorter separation, however, will increase the robustness of the solution. First of all, a larger number of GPS satellites will be jointly observed by both GPS receivers, leading to a reduced number of DGPS data outages and redundancy. Second, and more important, when using dual-frequency GPS receivers, the double difference integer carrier-phase ambiguities can be determined with a much higher reliability due to the quasi elimination of the relative ionosphere, which dramatically strengthens the relative position solution.

3.3 Monostatic pursuit mode

In the monostatic pursuit mode of the TanDEM-X mission, the satellite formation has an along-track separation of 30–50 km, which can be represented by the baseline geometry sketched in Fig. 1. This means that spacecraft A at point P pursues spacecraft B at point Q with a time offset of $\Delta t \approx 4$–7 s. In this case, the interferometric baseline may be expressed as

$$\mathbf{B} = \mathbf{r}_{\mathrm{A}}(t_0 + \Delta t) - \mathbf{r}_{\mathrm{B}}(t_0) \tag{9}$$

which looks similar to the repeat-pass case according to Eq. 3.

Due to the relatively short inter-satellite separation, the relative spacecraft position could still be computed directly using DGPS data and with the same accuracy as described above. However, the baseline vector in Eq. 9 is not measured by DGPS. At any given time, t, the position of spacecraft A can be expressed as the position of spacecraft B and the observed relative spacecraft position $\Delta\mathbf{r}_{\mathrm{DGPS}}$ yielding

$$\mathbf{r}_{\mathrm{A}}(t) = \Delta\mathbf{r}_{\mathrm{DGPS}}(t) + \mathbf{r}_{\mathrm{B}}(t). \tag{10}$$

By combining Eqs. 9 and 10, the interferometric baseline at $t = t_0 + \Delta t$ now becomes

$$\mathbf{B} = \Delta\mathbf{r}_{\mathrm{DGPS}}(t_0 + \Delta t) + \mathbf{r}_{\mathrm{B}}(t_0 + \Delta t) - \mathbf{r}_{\mathrm{B}}(t_0), \tag{11}$$

which means that $\mathbf{r}_{\mathrm{B}}(t_0 + \Delta t) - \mathbf{r}_{\mathrm{B}}(t_0)$ yields an additional error due to absolute orbit reconstruction uncertainties between epochs t_0 and $t_0 + \Delta t$. For short time-intervals, the errors of the reduced dynamic satellite orbit have a high degree of temporal correlation, and thereby reduce the interferometric baseline error in this case to

$$\epsilon_{\mathbf{B}} = \epsilon_{\Delta\mathbf{r}}(t_0 + \Delta t) + \frac{\partial \epsilon_{\mathbf{r}}}{\partial t}\Delta t. \tag{12}$$

Analyzing the orbit data used to create Table 2, it was found that the orbital errors in each direction change over short periods of time with a maximum rate, $\partial\epsilon_{\mathbf{r}}/\partial t$, of 0.05 mm/s. For a maximum time interval of 8 s, this means a maximum error of 0.4 mm in the difference of the absolute GRACE positions for each component. Combining this with the average accuracy of the relative position solution, the resulting baseline will have a maximum mean 2D uncertainty

$$\sigma_{\mathrm{B}} = \sqrt{2\,(\bar{\sigma}^2_{T,\mathrm{DGPS}} + \sigma^2_{(\partial\epsilon/\partial t)\Delta t})} \tag{13}$$

of approximately 1.7 mm for a monostatic formation flight with a time offset of 8 s in the flight direction.

ALI is performed in the bistatic mode. The along-track separation is supposed to vary between 20 and 40 m for an X-band interferometer (Gill and Runge 2004), which corresponds to a temporal separation between roughly 2.5 and 5 ms. In this case, the error component $(\partial\epsilon_{\mathbf{r}}/\partial t)\Delta t$ may be neglected, which simplifies Eqs. 13 to 8. Gill and Runge (2004) have estimated a required relative position accuracy of 0.9 mm for X-band ALI, based on a 10° interferometric phase noise level. This requirement can be fulfilled by DGPS observations assuming the obtained GRACE σ_{T}-accuracy results listed in Table 3.

4 Performance analysis

To investigate and assess the baseline performance for the bistatic and monostatic pursuit mode under quasi-realistic conditions, i.e., to simulate the helical baseline rotation, we use the two orbit predictions for the tandem formation flight that are based on fully dynamic trajectory modeling (Sect. 2.4). The cross-track baseline vector, $\mathbf{B}_{\mathrm{RN}}$, can now be determined as a function of time since t_0 or the tilt angle α using both orbit predictions. The baseline estimate applies both for the bistatic and the monostatic case.

We will consider the estimated baseline uncertainty for the monostatic operational mode as the *worst case* for the performance assessment. In other words, if the monostatic baseline performance fulfills the required DEM accuracy, the same must be true for the bistatic case for which we expect a slightly decreased baseline standard deviation (see Sect. 3.2). The baseline error is propagated to topographic height errors using Eq. 30 in Appendix A. Note that locally induced height errors due to changes of terrain elevation are neglected. However, Eq. 30 can be used for a reliable priori performance estimation.

The results are plotted in Fig. 4. The estimated relative height error σ_{h} is expressed as function of radar look angle θ_{p} and the baseline length B, which is directly related to the tilt angle α due to baseline dynamics. θ_{p} is an independent parameter and was varied between 10 and 50° at each predicted epoch to account for varying geometric distortion effects induced by different terrains.

During the first quarter-rotation $\alpha \in [0°, 90°]$, the baseline contracts from 3,000 to 300 m (Fig. 4a). The induced height bias is always beneath the 1 m performance threshold up to a tilt angle of roughly $\alpha = 85°$. The bias raises slightly with increasing view angle. Figure 4a confirms the low-frequency modulation of the topographic height bias that would occur for an interferometric measurement using ScanSAR pairs of a maximal acquisition window (rectangle with bold lines).

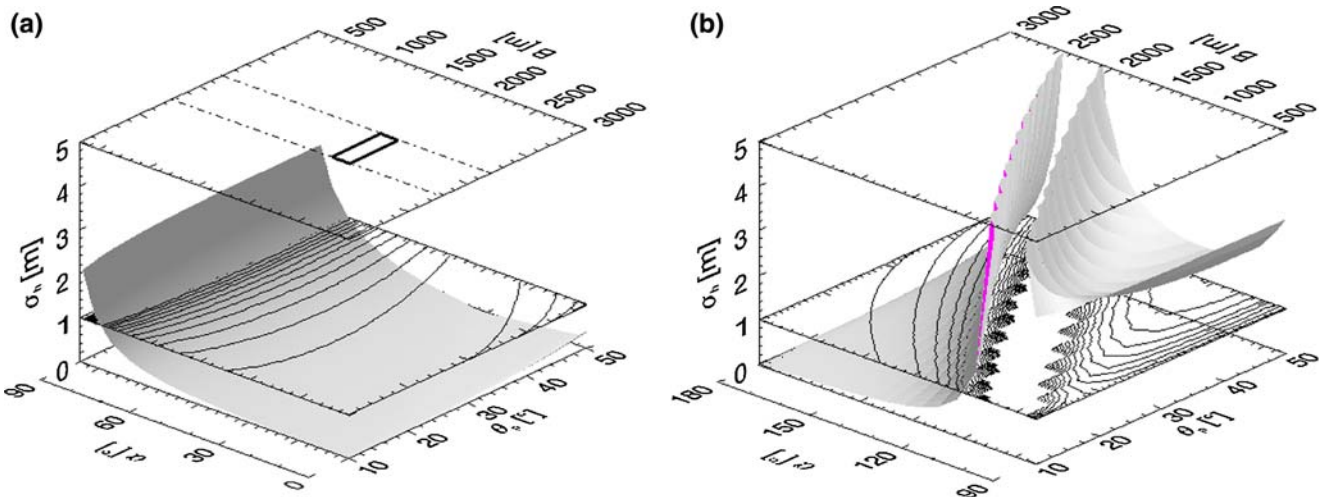

Fig. 4 3D plots of relative topographic height errors σ_h as a function of the radar look angle θ_p and the baseline length B in case of the monostatic pursuit mode. **a** Estimated performance for baseline attitudes $\alpha \in [0°, 90°]$ assuming a mean satellite altitude of H=520 km and a mean baseline standard deviation of σ_B = 1.7 mm. The plane of isolines at σ_h = 1 m indicates the performance threshold derived from the DTED-3 specifications. The *dash-dotted lines* in the upper coordinate frame represent the 100 km on-ground ScanSAR swath at a mid-swath radar look angle of $\theta_p = 30°$. The *rectangle with bold lines* delimits the corresponding maximum size ($100 \times 3,000$) of terrain which can be mapped by a single ScanSAR data take. **b** Estimated relative height errors for baseline attitudes $\alpha \in (90°, 180°]$. The rupture in the surface is caused by the singularity occurring at $\theta_p - \alpha = 90°$

In the second quarter-rotation $\alpha \in (90°, 180°]$, the baseline extends from 300 to 3,000 m (Fig. 4b). Here, the performance is mostly corrupted by the singularity event at $\theta_p - \alpha = 90°$. Only the noise levels occurring for baseline lengths $B \in [800\,\text{m}, 3{,}000\,\text{m}]$ at $\theta_p = 10°$ and $B \in [2{,}500, 3{,}000\,\text{m}]$ at $\theta_p = 50°$ are tolerable.

To assess the baseline performance, the estimated height bias in each DEM point p is related to the corresponding height ambiguity h_a, which is also a function of the parameters B, θ_p and α. It can be formulated as

$$h_a = \left| \frac{\lambda\, H_p}{m\, B_{\perp,p}} \tan\theta_p \right| \quad m = 1, 2 \tag{14}$$

with the effective baseline $B_{\perp,p} = B\cos(\theta_p - \alpha)$, and where λ denotes the radar wavelength (3.1 cm for X-band) and H_p the satellite's altitude above the terrain at target point P (see Fig. 5). The SAR acquisition parameter m has to be set to $m = 1$ for multistatic acquisition and to $m = 2$ for monostatic data takes.

Using the same baseline predictions as for the analysis in Fig. 4a and Eq. 14, we find the lowest height ambiguity $h_a \approx 1\,\text{m}$ for $\theta_p = 10°$, $B = 3,000\,\text{m}$ and the highest level $h_a \approx 73\,\text{m}$ for $\theta_p = 50°$, $B = 300\,\text{m}$. If the SAR data are acquired in the monostatic mode ($m = 2$), the height ambiguities are halved, which doubles the sensitivity of the interferometric measurement to topographic relief.

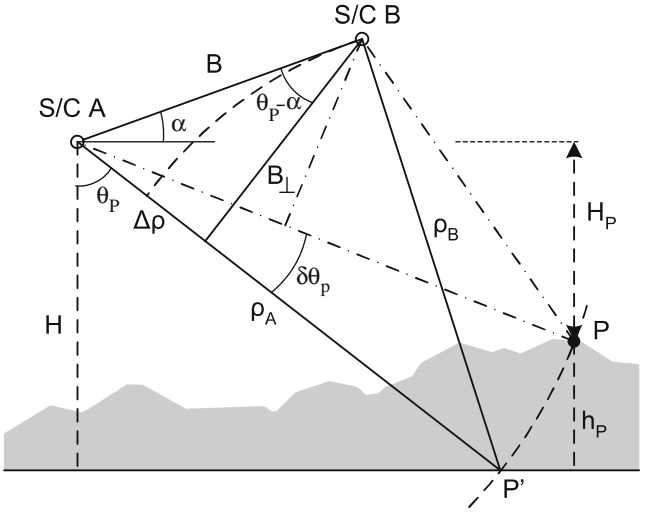

Fig. 5 Geometric configuration for SAR interferometry. Using the height H of spacecraft A above a reference surface, the range ρ_A and the baseline B, it is possible to estimate a topographic height h_p of target point P with respect to a point P' at the same range. H_p indicates the height of spacecraft A above the target point P

5 Discussion

Our analysis clearly reveals the antagonistic behavior of the estimated height accuracy to various performance parameters: At a certain view angle, the purely baseline-induced height bias, for example, increases as the interferometric phase-induced sensitivity to relief decreases and vice versa. Taking a certain baseline attitude, the noise level slightly drops with steeper view angles, while perturbing geometric effects due to terrain elevations may accumulate. Mapping a mountainous region with a steep view angle (small θ_p) leads to geometric problems such as foreshortening and layover, which make reliable phase unwrapping more difficult. In contrast, a shallow look angle (e.g. 45° for SRTM) creates data gaps due the effect of shadowing.

These geometric problems can be solved by the approach of multibaseline SAR interferometry (Ferretti et al. 1997) and by using a reference DEM. On the one hand, the use of multiple interferograms of the same scene increases the height ambiguity level. On the other hand, the combination of ascending and descending SAR data-takes will help to overcome the geometric problems for phase unwrapping and thus improve the quality. Another performance parameter is the critical effective baseline, $B_{\perp}^{\mathrm{crit}}$, beyond which complete geometric (baseline) decorrelation occurs since the spectral shift exceeds the pulse bandwidth (Gatelli et al. 1994). To ensure geometrically well-correlated interferograms, the effective baseline for topography estimation should always be smaller than $\sim 0.7 B_{\perp}^{\mathrm{crit}}$ (Hanssen 2001).

For a multistatic SAR interferometer, however, volume decorrelation may have a substantial impact on the achievable height accuracy (Krieger et al. 2003). This effect is mainly caused by different penetration and backscattering characteristics of SAR signals in vegetation. Furthermore, Doppler decorrelation will become an inherent problem of co-registered SAR images acquired in a formation flight with a selectable along-track separation between transmitter and receiver. This error source is caused by a misfit of the joint antenna footprint, i.e., a difference in the Doppler centroid frequencies Δf_{DC}. Therefore, an appropriate azimuth filtering of the interferometric channels should be applied accounting for variable along-track baselines.

One of the most important merits of a (single-pass) multistatic SAR interferometer is its capability to acquire SAR images quasi-simultaneously, which overcomes the problem of temporal decorrelation and allows the cancellation of atmospheric/ionospheric phase contributions in the interferogram. Repeat-pass interferometry is usually applied to measure changes in the Earth's surface, especially to measure surface displacements within a certain time interval (Massonnet and Feigl 1998). The standard approach is to subtract the topographic phase information from the interferometric measurement by using a reference DEM. The result is a *differential* interferogram that basically records the deformation field occurring between the acquisition epochs t_1 and t_2.

Along with the disturbing phase contributions coming from baseline uncertainties and the atmosphere/ionosphere, mismodeled topography will also contribute to the noise in the differential interferogram. Furthermore, the reference DEM used for topographic correction does not precisely reproduce the status of the relief at acquisition epoch t_1, which is a special problem for a rapidly changing surface like an ice shelf.

Utilizing the performance of a multistatic SAR mission like TanDEM-X, the concept of three-pass differential interferometry, as demonstrated by Zebker et al. (1994b), may be applied to counteract this problem. At the single-pass epoch t_0, high-precision topography can be estimated using the bistatic and atmospheric-free pair of points P and Q (cf. Fig. 1). Then, the deformation field can be measured by using the third SAR data-take at repeat-pass epoch t_2 and the monostatic SAR acquisition of point Q. Only the deformation pair will be affected by the atmosphere/ionosphere and the coherence will degrade due to temporal decorrelation.

Since only spacecraft A will acquire the SAR deformation pair, the repeat-pass baseline has to be estimated using absolute orbit solutions for spacecraft A, which significantly increases the baseline-induced phase noise. The standard approach is to subtract a linear 'phase ramp' from the interferometric measurement, which distorts or even removes the deformation signals of low-frequency modulations. These signals are of great interest for geophysical research, since postseismic relaxation and postglacial rebound of the lithosphere have to be measured for a slow vertical rate ($\sim$1 mm year^{-1}) and for a long duration (10^1–10^3 year) (Massonnet and Feigl 1998). To evaluate the interferometric baseline performance, both for the topographic and the deformation pair prior to DEM generation, an SRTM DEM could be used for a priori topographic correction.

In case of the bistatic (differential) interferogram, the residual phase pattern will be purely orbital, down to the accuracy level of the reference DEM, whereas the one for the repeat-pass interferogram will be orbital and atmospheric. However, if relative positioning with DGPS works well, the height bias caused by the bistatic baseline will be much lower than the one of an SRTM DEM. The stated objective for SRTM's relative vertical accuracy is $<$10 m linear error at 90% probability (DTED-2 specification).

Applying an orbital adjustment approach, as recently demonstrated by Kohlhase et al. (2003), may help to perform a posteriori correction of the baseline estimates. This technique is based on the measurement of baseline-induced phase gradients in well-correlated 'pre-fit' interferograms to estimate orbital adjustment components assuming a dominant orbital phase screen (OPS). This approach has yielded mean standard deviations for normal and radial adjustment components in the same order of magnitude as the ones listed in Table 2. Consequently, the use of reduced dynamic orbit determination techniques, as presented by Montenbruck et al. (2004), will also improve the baseline performance for repeat-pass interferometry.

6 Summary and conclusions

It has been proven that the estimated baseline performance of a multistatic SAR interferometer in a close-formation flight fulfills the DTED-3 relative height accuracy requirement ($<$2 m linear point-to-point error at 90% probability) for most of the baseline constellations if geodetic-grade dual-frequency GPS receivers onboard the SAR satellites are used for relative positioning. Note, however, that for the overall InSAR performance estimation, phase-noise-induced height errors have also to be analyzed and assessed, which come from temporal-, thermal-, geometrical-, and processing-induced decorrelation effects.

The assessment of realistic GPS POD results obtained from the GRACE mission has revealed a cross-track baseline accuracy of about 1.4 mm (2D 1σ) for a bistatic acquisition

mode with little or no along-track displacements, and about 1.7 mm for a monostatic acquisition mode with an along-track offset of 50 km. When using reduced dynamic orbit determination techniques, a GRACE trajectory has been reconstructed with a 3D mean standard deviation of about 5 cm, thus allowing the estimation of repeat-pass baselines with an accuracy level down to 4 cm (2D 1σ).

If a single-frequency GPS receiver is used for differential positioning, the direct elimination of differential ionospheric delay of the GPS signals is no longer possible. Furthermore, the resolution of the carrier-phase ambiguities is complicated and becomes even more difficult and inaccurate with increasing spatial separation. Therefore, the performance of the processing scheme using code pseudorange and carrier-phase measurements of only one GPS signal must be investigated with respect to varying and long baselines (i.e., >1 km). While encouraging results have been obtained using hardware-in-the-loop simulations for single-frequency GPS (Busse 2003; Leung and Montenbruck 2005), it is not yet clear to what extent the achieved millimeter level can be realized in a real space mission.

Although we believe that the dual-frequency GPS baseline performance will also fulfill the DTED-3 horizontal accuracy requirements, a further analysis should clarify the propagation of the total 3D baseline error vector to the height and horizontal circular bias.

Finding a correct trade-off between a low topographic height bias, good coherence of the SAR data, and optimal terrain circumstances such as relief, vegetation, as well as temporal decorrelation will be the main objective for the planning of a future multistatic SAR mission. Using a dual-frequency GPS receiver as an operational tool for POD and relative navigation will help to solve most problems related to a formation flight in a low Earth orbit (LEO) and ensure that the 2D baseline accuracies are less than 2 mm.

Acknowledgements The authors would like to thank Oliver Montenbruck from the DLR German Space Operations Center for his valuable comments on the manuscript. Discussions with Gerhard Krieger from the DLR Microwaves and Radar Institute are greatly appreciated. Furthermore, the authors would like to thank two anonymous reviewers for helpful comments and suggestions. The study presented in this article has mainly been carried out in the framework of a recently finished research fellowship awarded by the Deutsche Forschungsgemeinschaft (DFG). The first author gratefully acknowledges this grant.

Appendix A: Propagation of baseline errors to height errors

Although the propagation of a baseline uncertainty to a topographic height error has already been derived by, e.g., (Rodriguez and Martin 1992; Zebker and Goldstein 1986), we would like to give a comprehensive description of the derivation, which is the essential approach for the performance analysis in this paper.

Figure 5 depicts the main principle of SAR interferometry. It is obvious that the height difference between two points at the same range cannot be resolved in a single SAR image, since they are mapped in one resolution cell. However, if the complex response of same points are observed from slightly different positions in space, separated by the baseline **B**, the change in view angle, $\delta\theta_\mathrm{p}$, can be determined from the change in the interferometric phase. Consequently, the interferometric phase measurement in range direction means measuring cumulative angular differences between neighboring resolution cells.

The height H of spacecraft A above a reference body and its range ρ_A to a target point P are assumed to be known so that the topographic height h_p of point P above the reference body can be expressed as

$$h_\mathrm{p} = H - \rho_\mathrm{A}\cos\theta_\mathrm{p}. \tag{15}$$

By introducing the tilt angle α, h_p can be extended to

$$\begin{aligned} h_\mathrm{p} &= H - \rho_\mathrm{A}\cos(\alpha+\theta_\mathrm{p}-\alpha) \\ &= H - \rho_\mathrm{A}\left[\cos\alpha\sqrt{1-\sin^2(\theta_\mathrm{p}-\alpha)} - \sin\alpha\sin(\theta_\mathrm{p}-\alpha)\right]. \end{aligned} \tag{16}$$

In Eq. 16, the dependency from the baseline cannot explicitly be seen. Henceforth, we have to find a function $f(B)$ that relates the baseline attitude parameter $\theta_\mathrm{p}-\alpha$ with the baseline length. To estimate a height error induced by a baseline uncertainty, h has to be derived with respect to B, thus

$$\frac{\partial}{\partial B}h(B) = \frac{\partial h}{\partial f(B)} \bullet \frac{\partial f(B)}{\partial B}. \tag{17}$$

Theorem *A function* $f : B \to f(B);\ B \in \mathbb{R}_+$ *exists that obeys the relation*

$$f(B) := \sin(\theta_\mathrm{p}-\alpha), \quad \left(0 < \theta_\mathrm{p} < \frac{\pi}{2}, 0 \le \alpha < \pi\right) \tag{18}$$

Proof The measured interferometric phase for resolution cell P can be expressed as

$$\begin{aligned} \Phi_\mathrm{p} &= \varphi_\mathrm{Ap} - \varphi_\mathrm{Bp} = -\frac{2m\pi}{\lambda}(\rho_\mathrm{A}-\rho_\mathrm{B}) \\ &= -\frac{2m\pi}{\lambda}\left[\rho_\mathrm{A} - \sqrt{\rho_\mathrm{A}^2 + B^2 + 2B\rho_\mathrm{A}\sin(\theta_\mathrm{p}-\alpha)}\right] \end{aligned} \tag{19}$$

where

$$\Delta\rho = \rho_\mathrm{A} - \sqrt{\rho_\mathrm{A}^2 + B^2 + 2B\rho_\mathrm{A}\sin(\theta_\mathrm{p}-\alpha)} \tag{20}$$

is the true and non-linear expression for the range difference in the line of sight. Note that the theoretical situation, such as the one sketched in Fig. 5, can never occur since it is not possible to uniquely estimate the height difference between points P and P' from the interferometric phase change $\delta\Phi$.

In the far-field theory (Zebker and Goldstein 1986), the path-length difference $\Delta\rho$ may be approximated by

$$\Delta\rho = B\sin(\theta_\mathrm{p} - \alpha) = B_{||} \tag{21}$$

simplifying Eq. 19 to

$$\Phi_\mathrm{p} = -\frac{2m\pi}{\lambda} B\sin(\theta_\mathrm{p} - \alpha). \tag{22}$$

After transformation, we find

$$\sin(\theta_\mathrm{p} - \alpha) = -\frac{\lambda\ \Phi_\mathrm{p}}{2m\pi\ B} := f(B). \tag{23}$$

Equation 17 can now be re-written as

$$\frac{\partial}{\partial B}h(B) = \frac{\partial h}{\partial\sin(\theta_\mathrm{p} - \alpha)} \bullet \frac{\partial\sin(\theta_\mathrm{p} - \alpha)}{\partial B}. \tag{24}$$

Building the first partial derivative

$$\begin{aligned}\frac{\partial h}{\partial f(B)} &= \rho_\mathrm{A}\left[\frac{\cos\alpha\sin(\theta_\mathrm{p} - \alpha)}{\sqrt{1 - \sin^2(\theta_\mathrm{p} - \alpha)}} - \sin\alpha\right] \\ &= -\rho_\mathrm{A}\left[\frac{\sin\alpha\cos(\theta_\mathrm{p}-\alpha) - \cos\alpha\sin(\theta_\mathrm{p}-\alpha)}{\cos(\theta_\mathrm{p}-\alpha)}\right] \\ &= \rho_\mathrm{A}\frac{\sin\theta_\mathrm{p}}{\cos(\theta_\mathrm{p} - \alpha)}\end{aligned} \tag{25}$$

and the second partial derivative

$$\frac{\partial f(B)}{\partial B} = \frac{1}{B} \bullet \frac{\lambda\ \Phi_\mathrm{p}}{2m\pi\ B} = -\frac{1}{B}\sin(\theta_\mathrm{p} - \alpha) \tag{26}$$

yields the final expression

$$\frac{\partial h}{\partial B} = -\frac{\rho_\mathrm{A}}{B}\tan(\theta_\mathrm{p} - \alpha)\sin\theta_\mathrm{p} \quad \left(0 < \theta_\mathrm{p} - \alpha \leq \pi \ni \frac{\pi}{2}\right) \tag{27}$$

after multiplication.

It is evident that Eq. 27 becomes infinite for the baseline attitude $\theta_p - \alpha = \pi/2$. This means that the interferometric measurement is not possible since the baseline is aligned in the line of sight and one SAR instrument covers the other one. On the other hand, the influence of a baseline error vanishes if the baseline is exactly perpendicular to the line of sight ($\theta_\mathrm{p} - \alpha = 0$). This reveals that the height accuracy is very sensitive to the attitude of the baseline.

Assuming a flat terrain, the propagation of an error in the baseline to an error in the topographic height difference of a certain pixel may now be formulated as a 1σ standard deviation

$$\sigma_\mathrm{h} = \left|-\frac{\rho_\mathrm{A}}{B}\tan(\theta_\mathrm{p} - \alpha)\sin\theta_\mathrm{p}\right| \sigma_\mathrm{B}. \tag{28}$$

The height H_p of spacecraft A above the terrain at resolution cell P is known, and can be written as

$$H_\mathrm{p} = \rho_\mathrm{A}\cos\theta_\mathrm{p}. \tag{29}$$

Transformation and substitution yields

$$\sigma_\mathrm{h} = \left|-\frac{H_\mathrm{p}}{B}\tan(\theta_\mathrm{p} - \alpha)\tan\theta_\mathrm{p}\right| \sigma_\mathrm{B}. \tag{30}$$

□

References

Bamler R, Hartl P (1998) Synthetic aperture radar interferometry. Inverse Problems 14:R1–R54

Busse FD (2003) Precision formation-state estimation in low earth orbit using carrier differential GPS. PhD Dissertation, Dept of Aeronautics and Astronautics, Stanford University, Stanford

Case K, Kruizinga G, Wu S (2002) GRACE level 1B data product user handbook. JPL Publication D-22027, Jet Propulsion Laboratory, Pasadena

D'Amico S, Montenbruck O (2006) Proximity operations of formation flying spacecraft using an eccentricity/inclination vector separation. AIAA J Guidance, Control Dynamics (in press)

Evans NB, Lee P, Girard R (2002) The Radarsat 2&3 topographic mission: an overview. In: Proceedings of the international geoscience and remote sensing symposium (IGARSS), Toronto, June

Ferretti A, Prati C, Rocca F, Monti Guarnieri A (1997) Multibaseline SAR interferometry for automatic DEM reconstruction. In: Proceedings of the 3rd earth remote sensing (ERS) symposium, Florence, March

Fiedler H, Krieger G (2004) Close formation flight of passive receiving micro-satellites. In: Proceedings of the 18th international symposium on space flight dynamics (ISSFD), Munich, October

Gatelli F, Monti Guarnieri A, Parizzi F, Pasquali P, Prati C, Rocca F (1994) The Wavenumber shift in SAR Interferometry. IEEE Trans Geosci Remote Sensing 32(4):855–865

Gill E, Runge H (2004) Tight formation flying for an along-track SAR interferometer. Acta Astronaut 55:473–485

Goldstein RM, Zebker HA and Werner CL (1998) Satellite radar interferometry: Two dimensional phase unwrapping. Radio Sci 23(4):713–720

Haines B, Bertiger W, Desai S, Kuang D (2002) Initial orbit determination results for Jason-1: towards a 1-cm Orbit. Proc ION-GPS02, Portland

Hanssen RF (2001) Radar interferometry: data interpretation and error analysis. Kluwer, Dordrecht

Hoffmann-Wellenhoff B, Lichtenegger H, Collins J (2001) GPS theory and practice, 5th edn. Springer, Wien New York

IJssel J. van den, Visser P (2003) CHAMP Precise orbit determination using GPS data. Adv Space Res 31(8):1889–1895

Kohlhase AO, Feigl KL, Massonnet D (2003) Applying differential InSAR to orbital dynamics: a new approach for estimating ERS trajectories. J Geod 77:493–502, DOI 10.1007/s00190-003-0336-3

Krieger G, Fiedler H, Mittermayer J, Papathanassiou K, Moreira A (2003) Anaylsis of Multistatic Configurations for Spaceborne SAR Interferometry. Proc Radar Sonar Navigat 150(3):87–96

Krieger G, Moreira A, Hajnsek I, Hounam D, Werner M, Riegger S, Settelmeyer E (2004) A Tandem TerraSAR-X Configuration for Single-Pass SAR Interferometry. Proc RADAR04, Toulouse, October

Kroes R, Montenbruck O (2004) Spacecraft formation flying. GPS World 4:37–42

Kroes R, Montenbruck O, Bertiger W, Visser P (2004) Precise GRACE baseline determination using GPS. GPS Solutions 9:21–31, DOI 10.1007/s10291-0123-5

Leung S, Montenbruck O (2005) Real-time navigation of formation-flying spacecraft using global-positioning-system measurements. J Guidance Control Dynamics 28(2):226–235

Martin M, Klupar P, Kilberg S, Winter J (2001) TechSat 21 and revolutionizing space missions using microsatellites. Rep SSC01-1-3 of AIAA

Massonnet D, Feigl KL (1998) Radar interferometry and its applications to changes in the earth's surface. Rev Geophys 36:441–500

Massonnet D (2001) Capabilities and limitations of the Interferometric Cartwheel. IEEE Trans Geosci Rem Sensing 31(3):455–464

Montenbruck O, Gill E (2000) Satellite orbits: models, methods, and applications. Springer, Berlin Heidelberg New York

Montenbruck O, Kroes R (2003) In-flight performance analysis of the CHAMP BlackJack GPS Receiver. GPS Solutions 7:74–86, DOI 10.1007/s10291-003-0055-5

Montenbruck O, Van Helleputte T, Kroes R, Gill E (2004) Reduced dynamic orbit determination using GPS code and carrier measurements. Aerospace Sci Technol 9(3):261–271

Moreira A, Krieger G, Hajnsek I (2004) TanDEM-X: a TerraSAR-X Add-On satellite for single-pass SAR interferometry. In: Proceedings of the international geoscience and remote sensing symposium (IGARSS), Anchorage, September

Padia K, Mankad D, Chowdhury S, Majumder KL (2002) Digital elevation model generation using cross-track SAR-interferometry technique. Indian Cartographer MTQ-03:227–232

Parker TE, Matsakis D (2004) Time and frequency dissemation: advances in GPS transfer techniques. GPS World

Rodriguez E, Martin JM (1992) Theory and design of interferometric synthetic aperture radars. Proc IEE 139(2):147–159

NASA (2003) Studying the Earth's gravity from space: the gravity recovery and climate experiment (GRACE). NASA Facts, Rep FS-2002-1-029-GSFC, Goddard Space Flight Center, Maryland

Tapley BD, Bettadpur S, Ries JC, Thompson PF, Watkins M (2004a) GRACE measurements of mass variability in the Earth system. Science 305(5683):503–505

Tapley BD, Bettadpur S, Watkins M, Reigber C (2004b) The gravity recovery and climate experiment: mission overview and early results. Geophys Res Lett 31:L09607, doi:10.1029/2004GL019920

Werner M (2001) Shuttle Radar Topographic Mission (SRTM): mission overview. J Telecommun (Frequenz) 55(3–4):75–79

Werninghaus R, Balzer W, Buckreuss S, Mittermayer J, Mühlbauer P (2004) The TerraSAR-X mission. In: Proceedings of the European conference on synthetic aperture radar (EUSAR), Ulm, October

Zebker HA, Goldstein RM (1986) Topographic mapping from interferometric synthetic aperture radar observations. J Geophys Res 91(B5):4993–4999

Zebker HA, Farr T, Salazar R, Dixon T (1994a) Mapping the World's topography using radar interferometry: the TOPSAT mission. Proc IEEE 82(12):1774–1786

Zebker HA, Rosen PA, Goldstein RM, Gabriel A, Werner CL (1994) On the derivation of coseismic displacement fields using differential radar interferometry: the Landers earthquake. J Geophys Res 99:19617–19634

Zink M, Krieger G, Amiot T (2003) Interferometric performance of a Cartwheel constellation for TerraSAR-L. In: Proceedings of the Fringe03 Workshop, Frascati, December